Impact Electrochemistry of Layered Transition Metal Dichalcogenides

Chee Shan Lim,[†] Shu Min Tan,[†] Zdeněk Sofer,[‡] and Martin Pumera*[,†]

[†]Division of Chemistry & Biological Chemistry, School of Physical and Mathematical Sciences, Nanyang Technological University, 637371 Singapore and
[‡]Department of Inorganic Chemistry, University of Chemistry and Technology Prague, Technická 5, 166 28 Prague 6, Czech Republic

ABSTRACT Layered transition metal dichalcogenides (TMDs) exhibit paramount importance in the electrocatalysis of the hydrogen evolution reaction. It is crucial to determine the size of the electrocatalytic particles as well as to establish their electrocatalytic activity, which occurs at the edges of these particles. Here, we show that individual TMD (MoS_2, $MoSe_2$, WS_2, or WSe_2; in general MX_2) nanoparticles impacting an electrode surface provide well-defined current "spikes" in both the cathodic and anodic regions. These spikes originate from direct oxidation of the nanoparticles (from M^{4+} to M^{6+}) at the anodic region and from the electrocatalytic currents generated upon hydrogen evolution in the cathodic region. The positive correlation between the frequency of the impacts and the concentration of TMD nanoparticles is also demonstrated here, enabling determination of the concentration of TMD nanoparticles in colloidal form. In addition, the size of individual TMD nanoparticles can be evaluated using the charge passed during every spike. The capability of detecting both the "indirect" catalytic effect of an impacting TMD nanoparticle as well as "direct" oxidation indicates that the frequency of impacts in both the "indirect" and "direct" scenarios are comparable. This suggests that all TMD nanoparticles, which are electrochemically oxidizable (thus capable of donating electrons to electrodes), are also capable of catalyzing the hydrogen reduction reaction.

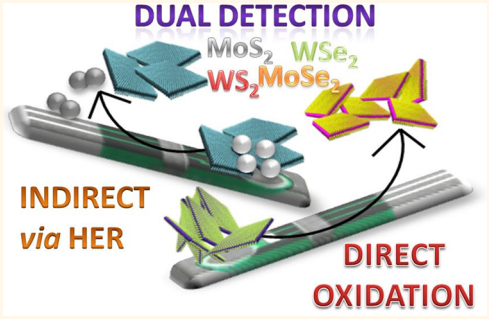

KEYWORDS: catalysis · hydrogen evolution · particle coulometry

Impact electrochemistry is a method enabling visualization of the electrochemical signal of a single nano/microparticle impacting a conductive surface.[1−4] It is somewhat analogous to the electrochemistry of a single molecule which, upon contact with a conductive surface (electrode), can be oxidized or reduced. A single collision results in the nano/microparticle being either adsorbed onto or rebounded off the electrode surface.[2] Such contact with the electrode surface may or may not lead to an electron transfer; it is largely dependent on the electrode material, applied potential, and nature of the particle. In the event of an electron transfer, there will be a transfer to/from electronic levels of the nano or microparticle instead of to/from molecular orbitals as in the case of a molecule.[4−6] This may result in either oxidation or reduction of the particle itself, or electrocatalysis (in terms of oxidation or reduction) of the molecule/ion present in the solvent.

Individual particle collision is a novel concept, which has been mainly developed by Compton and co-workers in the recent years.[1] It has been demonstrated that upon striking the electrode surface with sufficiently positive or negative potential, complete oxidation or reduction of a nanoparticle may occur.[7] Subsequently, one can quantify the number of atoms involved, the size of the nanoparticle as well as the size distribution in the colloid with high precision based on the charge passed during the collision event.[8] Deduction of other information such as concentration and particle type can be performed as well.[4] Such particle collision technique is largely based on a method called "particle coulometry".[8,9] "Direct" impact electrochemistry, a term coined for the oxidation or reduction of the nanoparticles themselves upon striking of an electrode surface, has been widely employed to determine the size of oxidizable metal and metal oxide nanoparticles such as gold, silver, copper, and molybdenum.[8,10−14] Recent studies have also extended the range of detectable nanoparticles to large organic nanoparticles based on indigo, C_{60},[15,16] as well as reducible species like Fe_3O_4.[17] Although other instrumental techniques such

* Address correspondence to pumera.research@gmail.com.

Received for review June 5, 2015 and accepted July 24, 2015.

Published online August 04, 2015
10.1021/acsnano.5b03357

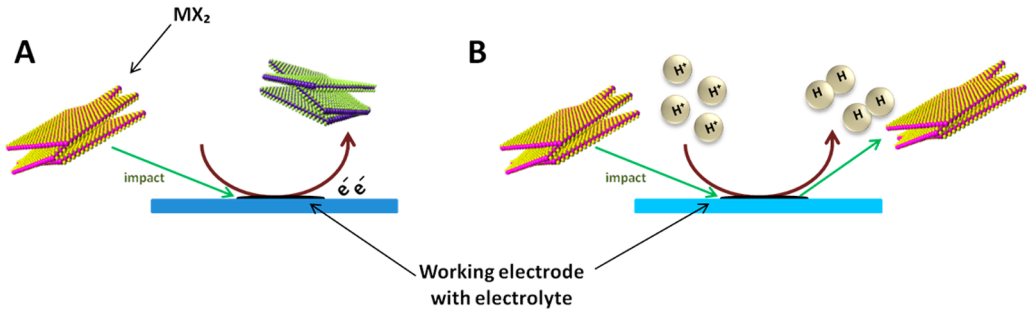

Figure 1. Schematic diagrams of (A) direct and (B) indirect voltammetry of impact nanoparticles of TMD (MX_2).

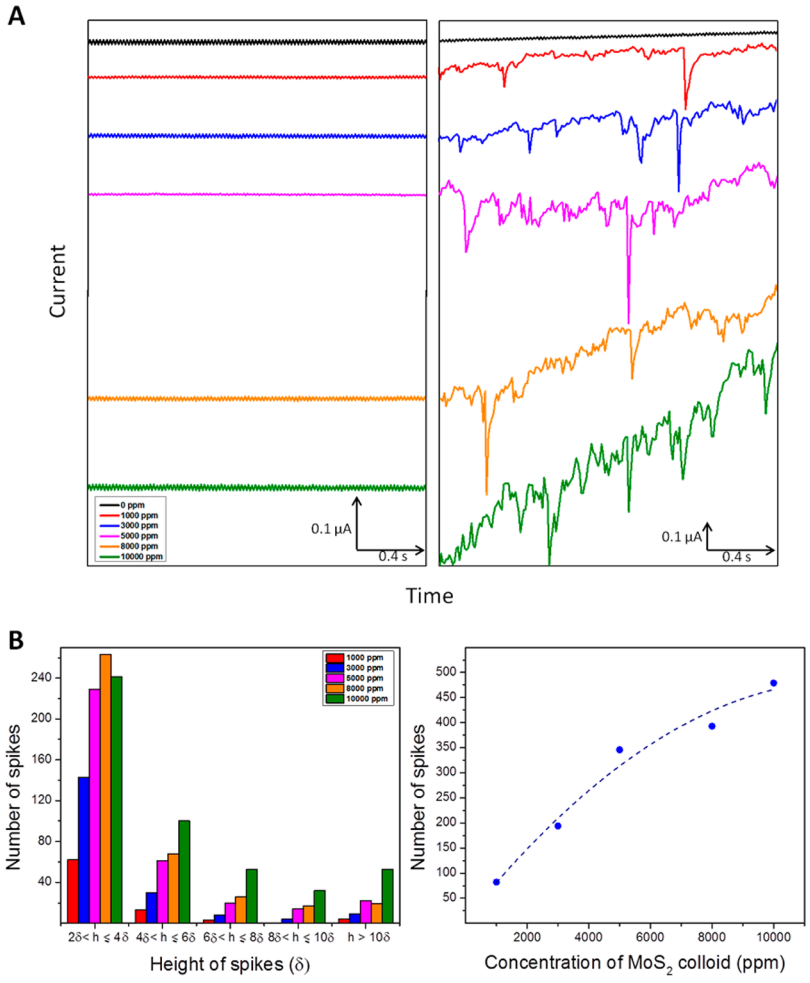

Figure 2. (A) Enlarged chronoamperograms of MoS_2 colloids in 0.5 M sulfuric acid at (left) −0.1 V and (right) −0.75 V (*vs* Ag/AgCl) over a 2-s interval, and (B) summary of spike count for various particle concentrations according to (left) amplitude and (right) quantity in the first 20 s.

as AFM and TEM also provide information about the type and size of particles,[18,19] the impact electrochemistry method is able to do so with high precision. This particle collision technique offers a sizable advantage in environmental monitoring, because the amount of nanoparticles released into the environment can be quantified *in situ*.[20,21]

Apart from "direct" voltammetry, there exists "indirect" voltammetry as well, which involves electrocatalysis of a surface reaction with nanoparticles. This voltammetry was first introduced by Micka,[22] before further development was demonstrated by Heyrovský and others,[23−25] where polarographic and voltammetric measurements of colloidal micro- and nanoparticles result in spikes obtained in polarograms and voltammograms. Heyrovský proposed that such spikes essentially originate from electrocatalytic currents of compounds present in the solution that have undergone catalysis following the striking of individual nanoparticles at the otherwise inert electrode surface.[24] Some of

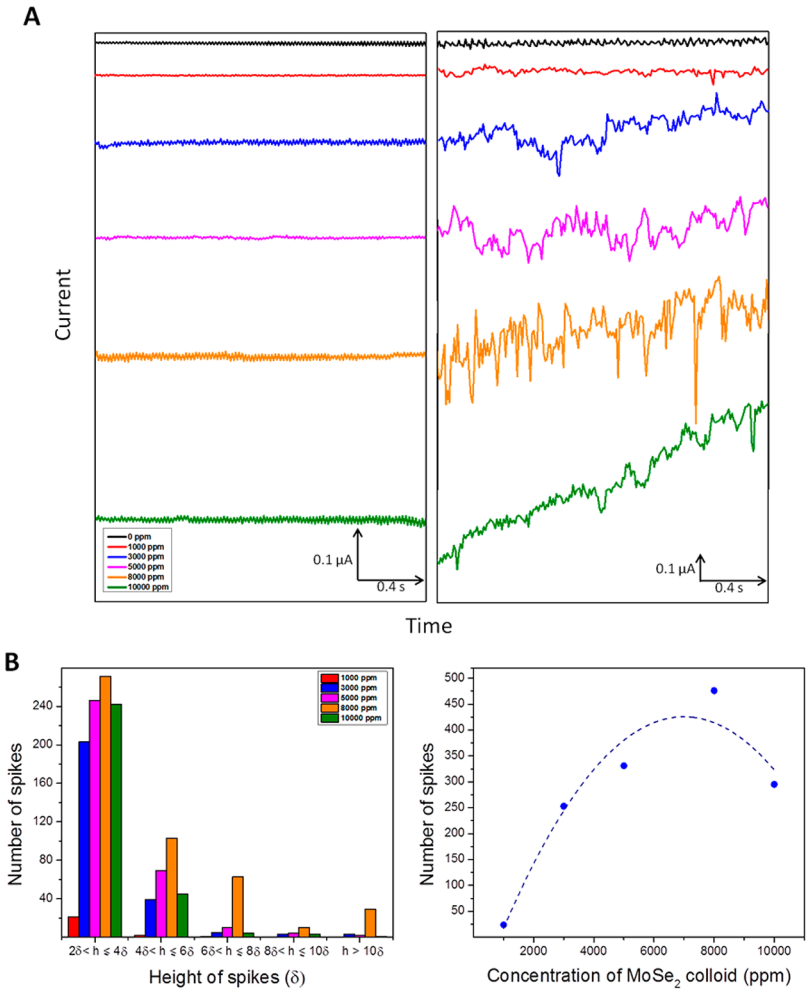

Figure 3. (A) Enlarged chronoamperograms of $MoSe_2$ colloids in 0.5 M sulfuric acid at (left) −0.1 V and (right) −0.8 V (*vs* Ag/AgCl) over a 2-s interval, and (B) summary of spike count for various particle concentrations according to (left) amplitude and (right) quantity in the first 20 s.

the particles include MnO_2, TiO_2, and SnO_2,[22−25] as well as metal powders, such as Mo, Ni, Fe, Cu, and Pt.[5,22,26−28] One of the common reactions electrocatalyzed by impacting particles is the hydrogen evolution reaction (HER; or proton reduction). The individual impact of a nanoparticle can catalyze and promote the reaction, which is otherwise kinetically slow at the surface of the electrode (*i.e.*, mercury or carbon electrode). It was further demonstrated that the frequency of the impacting particles catalyzing proton reduction increases with an increase in particle concentration in the suspension.[26]

In this work, we wish to further explore the practicality and suitability of this technique for the detection of individual particles of various layered transition metal dichalcogenides, including MoS_2, $MoSe_2$, WS_2, and WSe_2. The possibility of achieving the direct "coulometric" method as well as the indirect "electrocatalytic" method using a combination of both of the fundamentally different approaches is demonstrated in this work, as illustrated in Figure 1. In this work, we also demonstrate that all MX_2 nanoparticles, which are oxidizable, are also electrocatalytically active using the dual electrocatalytic/coulometric approach.

RESULTS AND DISCUSSION

Here, we demonstrate that impact electrochemistry of TMDs (MoS_2, $MoSe_2$, WS_2, and WSe_2) can be applied using both "direct" (inherent oxidation) and "indirect" (electrocatalytic) methods. "Indirect" impact electrochemistry was first performed *via* hydrogen evolution reactions. Similar to previous studies, the reduction of H^+ protons in acidic electrolyte occurs when the particles strike the electrode surface, which in turn results in the generation of current responses. It is important to note that the catalytic effect of the materials is only apparent after the onset of hydrogen evolution; onset potentials are largely dependent on the nanoparticles striking the electrode surface. The onset potential value for MoS_2, $MoSe_2$, and WS_2 is approximately −0.6 to −0.8 V *vs* Ag/AgCl (all potentials stated in this work are *vs* Ag/AgCl reference unless stated otherwise), as determined by previous studies, and the onset potential for WSe_2 is about −1.0 V *vs*

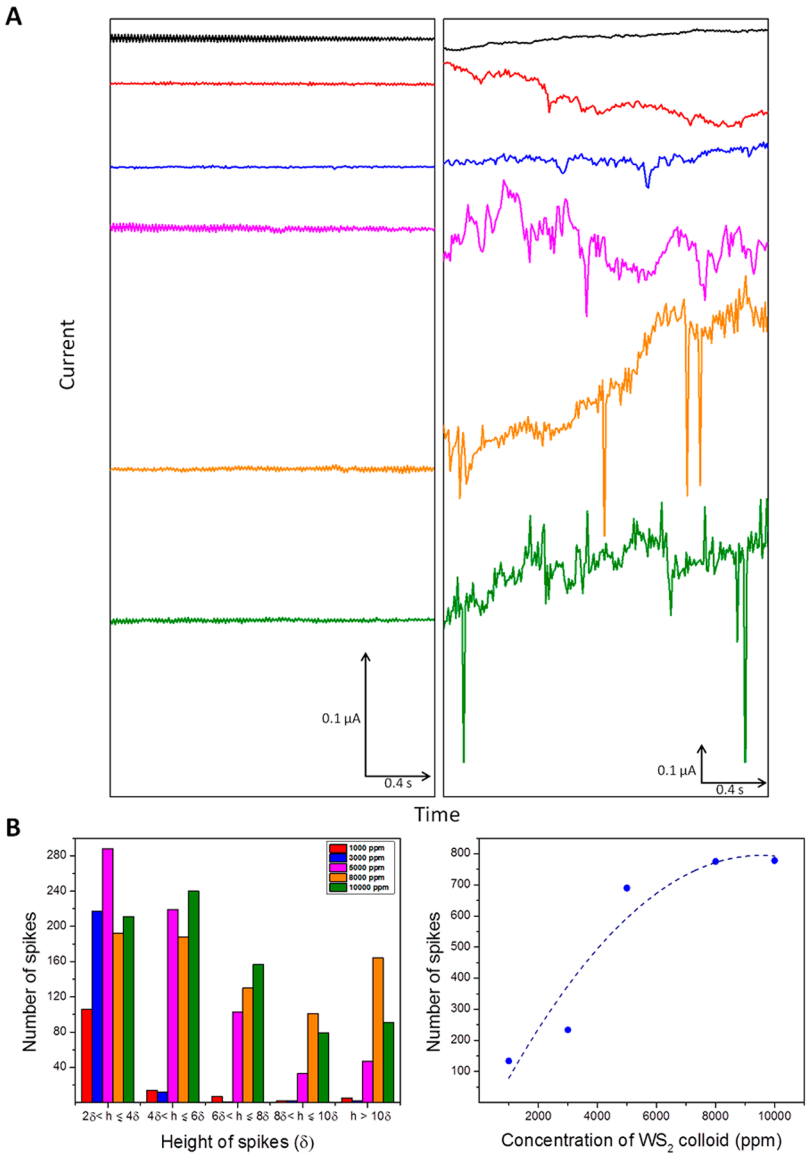

Figure 4. (A) Enlarged chronoamperograms of WS_2 colloids in 0.5 M sulfuric acid at (left) −0.1 V and (right) −0.9 V (*vs* Ag/AgCl) over a 2-s interval, and (B) summary of spike count for various particle concentrations according to (left) amplitude and (right) quantity in the first 20 s.

Ag/AgCl.[29] These values were used to select the potential of the chronoamperometric scans. Experiments were performed at two potentials for each material of various concentrations, one less negative than the onset of HER (fixed at −0.1 V for all materials) and one more negative than the onset.

Figure 2 illustrates the impacting of MoS_2 nanoparticles in sulfuric acid, which results in proton reduction. An enlarged view of the activity of the MoS_2 particles in a 2-s interval is shown in Figure 2A for clear observations of the impacts made. No visible HER spikes were observed at −0.1 V (*vs* Ag/AgCl), which is less negative than the onset potential of HER at MoS_2 (Figure 2A, left); only regular background signals were detected. In addition, a change in concentration of MoS_2 had negligible effect on the signals, implying that the surface reaction was not influenced by the particles at this stage. However, when the potential was fixed at −0.75 V, a value more negative than the onset of HER, random surges in the chronoamperograms were evident (Figure 2A, right). The amplitudes of the spikes for the different concentrations were considerably larger than for those without the nanoparticles (black line) at the same potential, clearly exhibiting the electrocatalytic behavior of the MoS_2 on HER. Comparison of the impacts produced by MoS_2 particles of various concentrations also shows increased frequency of successful impacts with increasing concentrations, further demonstrating the electrocatalytic activity of the MoS_2 particles. Full chronoamperograms over a 50-s interval are presented in the Supporting Information (Figure S1A).

With the catalytic effect of MoS_2 particles established, quantification of the spikes in the first 20 s was employed to further compare HER activity at various

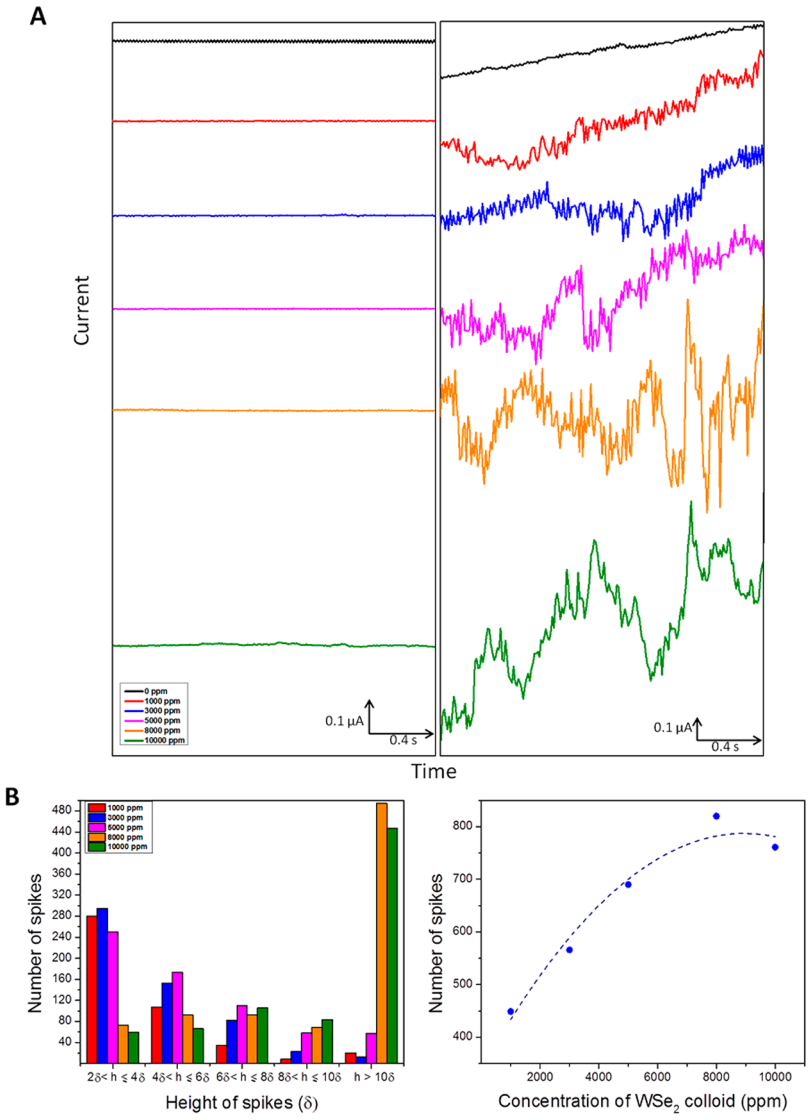

Figure 5. (A) Enlarged chronoamperograms of WSe_2 colloids in 0.5 M sulfuric acid at (left) −0.1 V and (right) −1.05 V (*vs* Ag/AgCl) over a 2-s interval, and (B) summary of spike count for various particle concentrations according to (left) amplitude and (right) quantity in the first 20 s.

catalyst concentrations. As illustrated in Figure 2B (left), the spikes were categorized according to amplitude, and only peaks at least twice the amplitude of the background signal (denoted by δ) were considered successful impacts. The average background signal was determined from the chronoamperogram obtained at −0.75 V with no MoS_2 particles present (black line, 0 ppm). For each category, a rise in concentration resulted in a general increase in the number of spikes. A significant observation is that fewer spikes were observed at larger amplitudes, and these larger amplitudes might be attributed to either the simultaneous impact of several particles leading to signal superposition, or the impact of a larger particle. The number of spikes was also plotted against nanoparticle concentration, as shown in the right panel of Figure 2B. It is evident that while HER was successfully catalyzed by MoS_2 nanoparticles *via* impact electrochemistry, the catalytic effect is also positively correlated with the concentration of particles.

Similar chronoamperometric profiles were observed when the potential of the $MoSe_2$ particles in catalyzing HER was examined, as illustrated in Figures 3A and S1B. Regular background responses were recorded before the onset of HER, but when the potential was fixed at a more negative value from the onset potential (−0.8 V), spikes were reflected in the chronoamperograms in a random manner. This is again indicative of the ability of the nanoparticles to catalyze the generation of molecular hydrogen. In contrast with MoS_2, the number of spikes recorded was not monotonic with increasing $MoSe_2$ concentration, where a maximum spike count was attained at 8000 ppm.

Spike quantification was subsequently carried out to confirm that 8000 ppm is indeed the concentration providing the highest spike frequency. Evidently, the

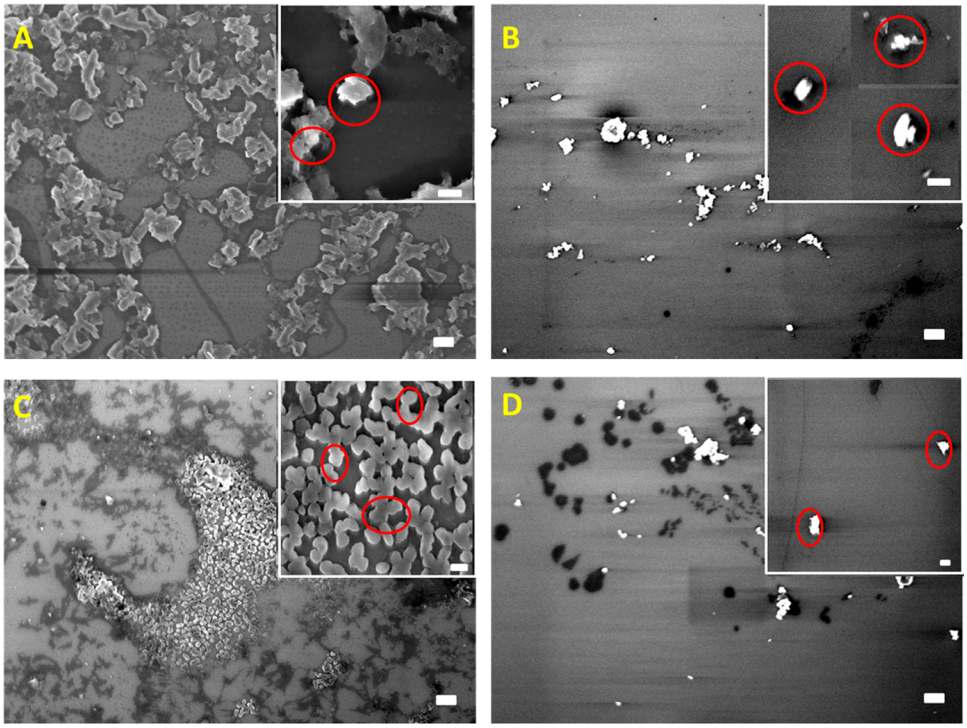

Figure 6. Scanning electron microscopy (SEM) images of (A) MoS_2, (B) $MoSe_2$, (C) WS_2, and (D) WSe_2 at 5000×, with scale bars representing 1 μm. Inset: SEM images of corresponding materials at 30 000×, with scale bars of 200 nm.

spike count for 8000 ppm of $MoSe_2$ exceeded that of other concentrations, as compared in Figure 3B. The trend of the number of spikes for different concentrations in each peak height category in the left panel of Figure 3B also remains consistent with the overall trend line shown on the right, where the number of spikes increased from 1000 ppm until a maximum was obtained at 8000 ppm, before experiencing a drop at 10 000 ppm. This occurrence can be explained by the tendency of particles to strike and then settle on the working electrode, resulting in a limited unoccupied area of the working electrode for new particles to strike. Conceivably, MoS_2 and $MoSe_2$ particles have comparable catalytic effect on HER judging from the overall spike counts recorded in Figures 2B and 3B. The only difference lies in the correlation between the concentration of particles and the frequency of collisions, which was more notable for MoS_2.

Further studies on the influence of nanoparticles on HER catalysis were also carried out using two other TMDs, WS_2 and WSe_2. Similar to the molybdenum counterparts, no significant spikes were observed at −0.1 V (Figures 4A and 5A, Figures S1C and S1D), which is less negative than the onset potential of HER. Spikes with varied amplitudes at irregular intervals were generated when the potentials were fixed at a point (−0.9 V and −1.05 V for WS_2 and WSe_2, respectively) after the occurrence of HER. These spikes indicate the successful catalyzing of HER upon impact of the WS_2 and WSe_2 nanoparticles, regarding them catalytic toward proton reduction. However, the spikes produced with the WS_2 particles are obviously more sharp and distinct as compared to WSe_2. A poorer catalytic performance can be suggested for the less distinguishable spikes obtained by WSe_2; this is supported by previous HER experiments carried out using voltammetric studies.[29]

Figures 4B and 5B summarize the amplitude and amount of spikes recorded for HER on each material. No major disparities were discovered for the total spike count of the two tungsten materials, and this observation is nearly identical to that for the molybdenum materials. The amplitudes of the spikes were relatively consistent with the predicted trend for WS_2, where fewer spikes were observed at higher amplitudes. In contrast, anomalies were present for the WSe_2 particles, more so for the 8000 and 10 000 ppm colloids. The number of spikes observed at amplitudes more than 10 times that of the background signal was unexpectedly more than half of the total number of spikes recorded. This inconsistency is likely due to the agglomeration of the nanoparticles at higher concentrations.

Performing impact electrochemistry using TMDs as catalysts for hydrogen evolution reaction affirmed that catalysis of the reaction is indeed affected by the nature, as well as the concentration of the nanoparticle applied. Analyses of the four TMDs showed conclusively that all of them possess some degree of catalytic activity toward HER. This is in line with previous studies conducted using traditional electrochemistry.[30−34] In addition, the general relationship between particle

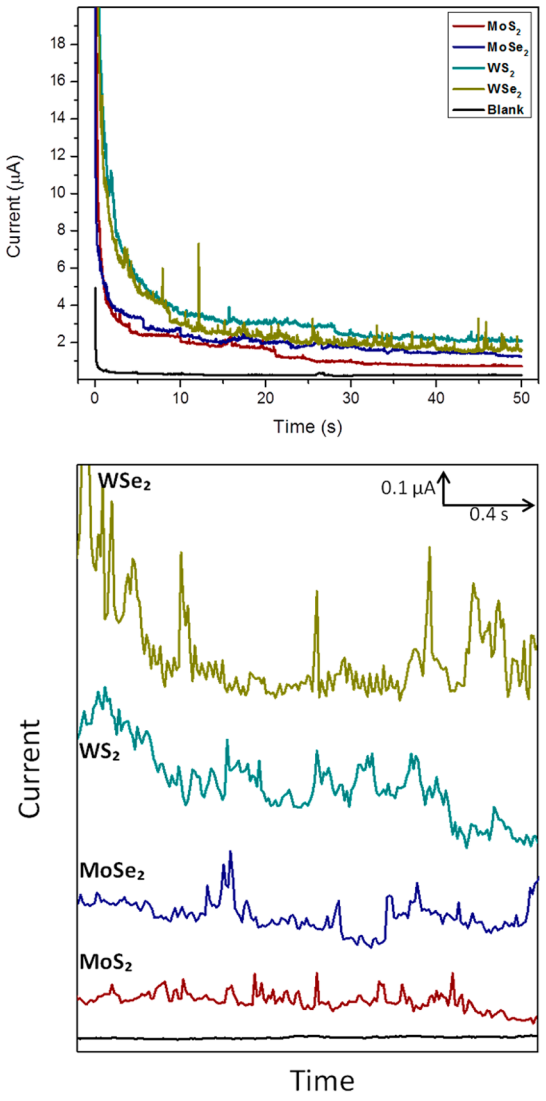

Figure 7. (Top) Chronoamperograms of oxidation of TMDs in 0.5 M sulfuric acid at +1.1 V (*vs* Ag/AgCl) and (bottom) enlarged version of scans over a 2-s interval.

concentration and spike frequency was also proven in the TMDs, with slight differences in the selenide particles where a concentration of 8000 ppm shows the best spike result. Peaks that are more distinct were also observed when proton reduction was carried out using MoS_2 and WS_2 particles. Finally, the trend in spike amplitude was more evident in the molybdenum species, despite more spikes recorded for HER using tungsten particles.

While "indirect" voltammetry was proven relatively successful using catalytic TMD nanoparticles, earlier applications of impact electrochemistry have only been established with small-sized nanoparticles[9] and have not been fully extended to particles of larger sizes. Because TMDs are larger, we wish to verify the viability of applying this concept to these particles by size determination performed *via* the inherent oxidation of these particles ("direct" voltammetry). The signals obtained were then evaluated to acquire experimental sizes of the particles, followed by comparison with the actual sizes detected using scanning electron microscopy (SEM).

SEM was performed on the TMD materials and, as displayed in Figure 6, the TMDs are not completely spherical metal nanoparticles due to their layered structures. MoS_2 contains platelet-like particles of various sizes; $MoSe_2$ particles possess uneven surfaces with a small degree of particle agglomeration. WS_2 particles appear to be rounder and more uniform than do the other TMDs, while WSe_2 exists as long, flat particles with uneven surfaces. Additional characterization including X-ray diffraction (XRD) and energy-dispersive X-ray spectroscopy (EDS) were also performed to determine the phase purity and presence of impurities in the TMDS respectively, as presented in the Supporting Information. As shown in Figure S2, the exfoliated MoS_2, WS_2 and WSe_2 are single phase compounds, while the $MoSe_2$ detected was in the form of Mo_3Se_4, suggesting a deficiency in selenium. This compound is formed upon vigorous exfoliation of lithium intercalated $MoSe_2$. Figures S3 and S4 show almost negligible amounts of impurities in the exfoliated TMDs other than carbon and oxygen which are likely attributed to the inadvertent presence of atmospheric carbon dioxide. Some of the other impurities detected include aluminum, titanium and iron; the trace amounts suggest that the impacts caused by the materials are largely dominated by the TMDs.

The size of the particles is a function of the charge passed with each spike.[3] By assuming a cube-like structural conformation for the TMDs, the edge length of the TMD particles that generated successful impacts can be evaluated using an equation (eq 1) slightly modified from a derivative of Faraday's law, as such:[8]

$$L = \sqrt[3]{\frac{QM_r}{\rho F z}} \qquad (1)$$

where Q is the amount of net charge passing through during a collision (denoted by the area under the spike recorded in the chronoamperograms minus the average background signal) and M_r is the relative molecular mass of the TMDs. ρ is the density of the TMDs, F is Faraday's constant (96 485 C/mol), and z is the number of electrons transferred. Here, two electrons are transferred during the oxidation, as suggested by Brookins and illustrated in the Supporting Information (Figure S5).[35] A general increase in the oxidation number of the metals from +4 to +6 is observed.

For size determination, oxidation was performed at +1.1 V for 50 s on 5000 ppm of all four TMDs, as illustrated in Figure 7. Six apparent oxidation signals were then chosen within a 2-s interval as the sample data set for all materials, and are illustrated in Figure 8.

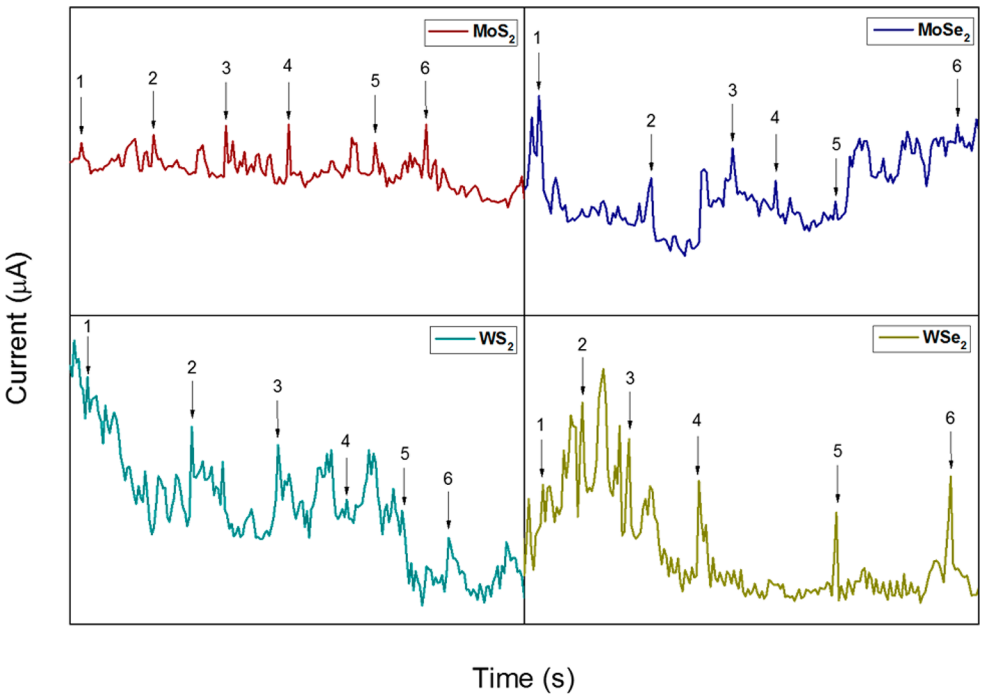

Figure 8. Spikes selected for size determination of the four materials under study.

The corresponding charge passed with each spike together with other relevant data required for size determination is summarized in Table S1 in the Supporting Information.

The particle edge size from each spike were also evaluated in Table S1. The average particle length for MoS_2, $MoSe_2$, WS_2, and WSe_2 are 496, 437, 439, and 775 nm, respectively, with slight deviations due to different particle sizes. This observation is also apparent in the SEM images in Figure 6 and images of some individual particles at higher magnification in the insets. In general, particles were observed to be approximately 400−600 nm in diameter. A comparison of the calculated values in Table S1 with the actual sizes obtained using SEM suggests that the determination of particle length using the spikes on the chronoamperograms is a relatively precise technique from the small discrepancies between the overall experimental and actual values. Among the four TMDs, size determination for MoS_2 appears to be the most accurate, accompanied by a small standard deviation of about 50 nm.

Nonetheless, there remain some deviations between the experimental and actual particle lengths because some spikes were evaluated to be the result of impact by nanoparticles larger than 600 nm. The variation of results can be attributed to the possible the coagulation of particles due to less effective separation in the electrolyte. In addition, cube-like conformation of the nanoparticles might not be the most accurate assumption for size determination. As a result, a assumption of spherical shape was further applied with a modified equation. The results are presented in the Supporting Information (Table S2 and eq S1); the evaluated particle radii are about half that derived from the cube-like hypothesis. Because particle size is largely dependent on the shape used for size determination, it is highly possible that the layered TMDs take on other shapes including cuboid-like or platelet-like morphologies. This undoubtedly poses challenges in the accuracy of size determination. Other than particle shape, larger particles (a few μm) were also not prominent in the recorded spikes. This might be indicative of the detection range of this technique. Despite the abovementioned limitations, this technique appears to be a viable method for size determination of particles even on a scale exceeding that achieved by prior studies, suggesting an upper detection limit of about 100 nm.[9] This finding serves as further testament to the high precision promised in earlier studies, although the shape and structure of the particles remain a crucial factor for consideration.

Finally, we examined whether the MX_2 nanoparticles can only electrocatalyze HER (without being oxidized themselves) or be oxidized directly (without electrocatalyzing HER). This investigation is significant for understanding the hydrogen evolution reaction using MX_2-based electrodes. Comparisons were drawn between the spike quantification of the "direct" (oxidation) and "indirect" (proton reduction) voltammetric studies at a particle concentration of 5000 ppm for each MX_2 nanoparticle material, as illustrated in Figure 9. The bi-directional reactions exhibited a general trend in which the number of nanoparticles catalyzing the HER process was comparable to the count of MX_2 NPs that were directly oxidizable.

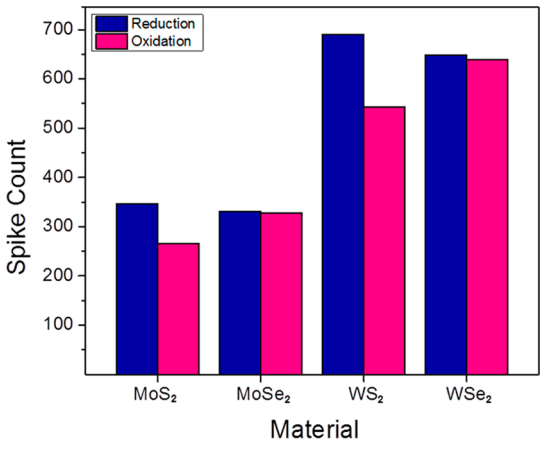

Figure 9. Total spike count in first 20 s for respective reactions using each material.

Therefore, most, if not all electrochemically oxidizable MX_2 nanoparticles are also catalytically active towards HER.

CONCLUSION

Impact electrochemistry has been in the frontier of electrochemical studies of nanoparticles in the past decade due to its convenience and high precision. Because it challenges other expensive methods of analysis, successful applications of this technique have been established for particle size determination as well as environmental monitoring. This work studied the particle collision of four transition metal dichalcogenides, which have been intensively discussed lately for their catalytic abilities. Hydrogen evolution reaction upon impact of these nanoparticles was successfully demonstrated along with comparisons between the catalytic functions of various materials and the catalytic behavior that occurs with changes in colloidal catalyst concentrations. Development of this technique can be promoted with other materials that are capable of catalyzing HER such as graphene derivatives and metal-based oxides. Apart from HER, the potential of applying this technique on other reactions including oxygen reduction or oxygen evolution can also be investigated subsequently. Further investigations of the practicality of this technique on TMDs were demonstrated by determining the size of the impacting particles upon oxidation and evaluating their dual functional behaviors. The concurrence of the impact electrochemistry-derived and actual scanning electron microscopy (SEM)-derived particle sizes, as well as the promising behaviors in both reduction and oxidation reactions, undoubtedly encourage further development of the practicability of this technique.

EXPERIMENTAL SECTION

Materials. Sulfuric acid (95−98%, v/v) was obtained from Sigma-Aldrich, Singapore. Bulk materials, MoS_2, WS_2, $MoSe_2$, and WSe_2 (<2 μm), and *tert*-butyllithium (1.7 M in pentane) were obtained from Sigma-Aldrich, Czech Republic. Hexane was obtained from Lach-ner, Czech Republic. Argon (99.9999% purity) was obtained from SIAD, Czech Republic. Three-E screen-printed electrodes (SPEs) of 3 mm working diameter were obtained from Zensor, Taiwan. Milli-Q water with a resistivity of 18.2 MΩ.cm was used throughout all experiments.

Apparatus. Scanning electron microscopy (SEM) was carried out on a silicon wafer with a Jeol 7600F SEM (Jeol, Japan) operating at 2 kV with a working distance of 5 mm to study the shape and diameter of the TMD particles dispersed in Milli-Q water. Energy-dispersive X-ray spectroscopy (EDS) was performed on the same equipment at 30 kV and a working distance of 15 mm to acquire the mapping and elemental composition of the TMDs.

All samples were analyzed by X-ray powder diffraction (XRD). Data collection was done with a Bruker D8 diffractometer in Bragg−Brentano parafocusing geometry. A Cu Kα radiation was used. Diffraction pattern were collected between 5° and 80° of 2θ. The obtained data were evaluated using Xpert HighScore 3.0e software.

Chronoamperometric studies were performed with a μAutolab type III electrochemical analyzer (Eco Chemie, The Netherlands) connected to a personal computer and controlled by NOVA 1.10 software. All voltammetry experiments were performed using the three-electrode system present on the SPEs, with an Ag/AgCl surface serving as the reference electrode and a platinum counter electrode surface around the working electrode surface. All electrochemical potentials in this report are stated *vs* the Ag/AgCl reference electrode.

Procedures. The exfoliated materials were obtained by stirring 3 g of the bulk powder in 20 mL of 1.7 M *t*-butyllithium in pentane for 72 h at 25 °C under an argon atmosphere. Suction filtration was then performed to separate the Li-intercalated compound from the excess intercalant and washed several times with hexane (dried over sodium). The Li-intercalated compound was then placed in water (100 mL) to obtain exfoliation and then centrifuged repeatedly (18 000*g*). The obtained material was dried in a vacuum oven at 50 °C for 48 h before further use.

Suspensions of the TMD particles were prepared in water, at 5 different concentrations of 1000, 3000, 5000, 8000, and 10 000 ppm. All chronoamperometry measurements were recorded at 10 ms intervals in 0.5 M sulfuric acid. The chronoamperometric potential before HER was fixed at −0.1 V, and at −0.75, − 0.80, − 0.90, and −1.05 V for MoS_2, $MoSe_2$, WS_2, and WSe_2 respectively, after the onset of HER. As for the "direct" voltammetry scans, the potential was fixed at +1.1 V.

Stock solutions of 20 000 ppm of the desired TMD and 1.0 M sulfuric acid were prepared first. The mixtures were subsequently diluted with water to obtain an overall TMD−acid−water suspension in the required concentration for the experiments. For measurement, the 3-component electrode was positioned in a horizontal manner before a fixed 50 μL of the suspension was drop casted onto the electrode surface. This experimental setup ensures that the impact of the particles is additionally guided by gravity besides simple Brownian motion. Chronoamperometry scans were carried out for 50 s immediately thereafter to detect all possible strikes of the particles onto the electrodes. To ensure accurate data collection, movement around the electrode was minimized during the scans. Chronoamperometry measurements were also carried out on blank solution containing only sulfuric acid as a reference for comparison. In this work, they are denoted as "0 ppm".

Acknowledgment. M.P. thanks the Ministry of Education, Singapore for Tier 2 grant ((MOE2013-T2 -1 -056). Z.S. was supported by Czech Science Foundation (GACR No. 15-07912S).

Conflict of Interest: The authors declare no competing financial interest.

Supporting Information Available: The Supporting Information is available free of charge on the ACS Publications website at DOI: 10.1021/acsnano.5b03357.

Full chronoamperograms of TMDs on 0.5 M sulfuric acid for HER electrocatalysis; Eh-pH diagrams for oxidation of TMDs at various potentials and pH; size determination of TMD nanoparticles assuming a cube-like conformation; size determination of TMD nanoparticles assuming a spherical conformation; equation used for spherical conformation. (PDF)

REFERENCES AND NOTES

1. Cheng, W.; Compton, R. G. Electrochemical Detection of Nanoparticles by 'Nano-Impact' Methods. *TrAC, Trends Anal. Chem.* **2014**, *58*, 79–89.
2. Rees, N. V. Electrochemical Insight from Nanoparticle Collisions with Electrodes: A Mini-review. *Electrochem. Commun.* **2014**, *43*, 83–86.
3. Rees, N. V.; Zhou, Y.-G.; Compton, R. G. Making Contact: Charge Transfer during Particle−Electrode Collisions. *RSC Adv.* **2012**, *2*, 379–384.
4. Pumera, M. Impact Electrochemistry: Measuring Individual Nanoparticles. *ACS Nano* **2014**, *8*, 7555–7558.
5. Korshunov, A. V.; Heyrovský, M. Voltammetry of Metallic Powder Suspensions on Mercury Electrodes. *Electroanalysis* **2006**, *18*, 423–426.
6. Korshunov, A.; Heyrovský, M.; Bakardjieva, S.; Brabec, L. Electrolytic Processes in Various Degrees of Dispersion. *Langmuir* **2007**, *23*, 1523–1529.
7. Dickinson, E. J. F.; Rees, N. V.; Compton, R. G. Nanoparticle-Electrode Collision Studies: Brownian Motion and the Timescale of Nanoparticle Oxidation. *Chem. Phys. Lett.* **2012**, *528*, 44–48.
8. Zhou, Y. G.; Rees, N. V.; Compton, R. G. The Electrochemical Detection and Characterization of Silver Nanoparticles in Aqueous Solution. *Angew. Chem., Int. Ed.* **2011**, *50*, 4219–4221.
9. Bartlett, T. R.; Sokolov, S. V.; Compton, R. G. Electrochemical Nanoparticle Sizing *via* Nano-Impacts: How Large a Nanoparticle Can be Measured? *ChemistryOpen* **2015**, 10.1002/open.201500061.
10. Qiu, D.; Wang, S.; Zheng, Y.; Deng, Z. One at a Time: Counting Single-Nanoparticle/Electrode Collisions for Accurate Particle Sizing by Overcoming the Instability of Gold Nanoparticles under Electrolytic Conditions. *Nanotechnology* **2013**, *24*, 505707.
11. Haddou, B.; Rees, N. V.; Compton, R. G. Nanoparticle−Electrode Impacts: The Oxidation of Copper Nanoparticles has Slow Kinetics. *Phys. Chem. Chem. Phys.* **2012**, *14*, 13612–13617.
12. Rees, N. V.; Zhou, Y.-G.; Compton, R. G. The Aggregation of Silver Nanoparticles in Aqueous Solution Investigated *via* Anodic Particle Coulometry. *ChemPhysChem* **2011**, *12*, 1645–1647.
13. Stuart, E. J. E.; Zhou, Y.-G.; Rees, N. V.; Compton, R. G. article-Impact Nanoelectrochemistry: A Fickian Model for Nanoparticle Transport. *RSC Adv.* **2012**, *2*, 12702–12705.
14. Giovanni, M.; Ambrosi, A.; Sofer, Z.; Pumera, M. Impact Electrochemistry of Individual Molybdenum Nanoparticles. *Electrochem. Commun.* **2015**, *56*, 16–19.
15. Cheng, W.; Zhou, X.-F.; Compton, R. G. Electrochemical Sizing of Organic Nanoparticles. *Angew. Chem., Int. Ed.* **2013**, *52*, 12980–12982.
16. Stuart, E. J. E.; Tschulik, K.; Batchelor-McAuley, C.; Compton, R. G. Electrochemical Observation of Single Collision Events: Fullerene Nanoparticles. *ACS Nano* **2014**, *8*, 7648–7654.
17. Tschulik, K.; Haddou, B.; Omanović, D.; Rees, N. V.; Compton, R. G. Coulometric Sizing of Nanoparticles: Cathodic and Anodic Impact Experiments Open Two Independent Routes to Electrochemical Sizing of Fe_3O_4 Nanoparticles. *Nano Res.* **2013**, *6*, 836–841.
18. Pyrz, W. D.; Buttrey, D. J. Particle Size Determination using TEM: A Discussion of Image Acquisition and Analysis for the Novice Microscopist. *Langmuir* **2008**, *24*, 11350–11360.
19. Boyd, R. D.; Pichaimuthu, S. K.; Cuenat, A. New Approach to Inter-Technique Comparisons for Nanoparticle Size Measurements; Using Atomic Force Microscopy, Nanoparticle Tracking Analysis and Dynamic Light Scattering. *Colloids Surf., A* **2011**, *387*, 35–42.
20. Stuart, E. J. E.; Reev, N. V.; Cullen, J. T.; Compton, R. G. Direct Electrochemical Detection and Sizing of Silver Nanoparticles in Seawater Media. *Nanoscale* **2013**, *5*, 174–177.
21. Stuart, E. J. E.; Tschulik, K.; Omanović, D.; Cullen, J. T.; Jurkschat, K.; Crossley, A.; Compton, R. G. Electrochemical Detection of Commercial Silver Nanoparticles: Identification, Sizing and Detection in Environmental Media. *Nanotechnology* **2013**, *24*, 444002.
22. Micka, K. Depolarisation der quecksilbertropfelektrode durch suspensionen unlöslicher stoffe IV. Suspensionen von mangandioxid. *Collect. Czech. Chem. Commun.* **1965**, *30*, 235–245.
23. Heyrovský, M.; Jirkovský, J. Polarography and Voltammetry of Ultrasmall Colloids: Introduction to a New Field. *Langmuir* **1995**, *11*, 4288–4292.
24. Heyrovský, M.; Jirkovský, J.; Štruplová-Bartáčková, M. Polarography and Voltammetry of Aqueous Colloidal TiO_2 Solutions. *Langmuir* **1995**, *11*, 4300–4308.
25. Heyrovský, M.; Jirkovský, J.; Müller, B. R. Polarography and Voltammetry of Aqueous Colloidal SnO_2 Solutions. *Langmuir* **1995**, *11*, 4293–4299.
26. Xiao, X.; Bard, A. J. Observing Single Nanoparticle Collisions at an Ultramicroelectrode by Electrocatalytic Amplification. *J. Am. Chem. Soc.* **2007**, *129*, 9610–9612.
27. Korshunov, A.; Heyrovský, M.; Bakardjieva, S.; Brabec, L. Electrolytic Processes in Various Degrees of Dispersion. *Langmuir* **2007**, *23*, 1523–1529.
28. Zhou, Y.-G.; Rees, N. V.; Compton, R. G. Electrochemistry of Nickel Nanoparticles is Controlled by Surface Oxide Layers. *Phys. Chem. Chem. Phys.* **2013**, *15*, 761–763.
29. Ambrosi, A.; Sofer, Z.; Pumera, M. 2H → 1T Phase Transition and Hydrogen Evolution Activity of MoS_2, $MoSe_2$, WS_2 And WSe_2 Strongly Depends on the MX_2 Composition. *Chem. Commun.* **2015**, *51*, 8450–8453.
30. Eng, A. Y. S.; Ambrosi, A.; Sofer, Z.; Šimek, P.; Pumera, M. Electrochemistry of Transition Metal Dichalcogenides: Strong Dependence on the Metal-to-Chalcogen Composition and Exfoliation Method. *ACS Nano* **2014**, *8*, 12185–12198.
31. Yang, Y.; Fei, H.; Ruan, G.; Xiang, C.; Tour, J. M. Edge-Oriented MoS2 Nanoporous Films as Flexible Electrodes for Hydrogen Evolution Reactions and Supercapacitor Devices. *Adv. Mater.* **2014**, *26*, 8163–8168.
32. Saadi, F. H.; Carim, A. I.; Velazquez, J. M.; Baricuatro, J. H.; McCrory, C. C. L.; Soriaga, M. P.; Lewis, N. S. *Operando* Synthesis of Macroporous Molybdenum Diselenide Films for Electrocatalysis of the Hydrogen-Evolution Reaction. *ACS Catal.* **2014**, *4*, 2866–2873.
33. Lin, J.; Peng, Z.; Wang, G.; Zakhidov, D.; Larios, E.; Yacaman, M. J.; Tour, J. M. Enhanced Electrocatalysis for Hydrogen Evolution Reactions from WS2 Nanoribbons. *Adv. Energy Mater.* **2014**, *4*, 1301875.
34. Velazquez, J. M.; Saadi, F. H.; Pieterick, A. P.; Spurgeon, J. M.; Soriaga, M. P.; Brunschwig, B. S.; Lewis, N. S. Synthesis and Hydrogen-Evolution Activity of Tungsten Selenide Thin Films Deposited on Tungsten Foils. *J. Electroanal. Chem.* **2014**, *716*, 45–48.
35. Brookins, D. G. *Eh-pH Diagrams for Geochemistry*; Springer-Verlag: Berlin, 1988; pp 104−107.